

Further explorations of Skyrme-Hartree-Fock-Bogoliubov mass formulas. IX: Constraint of pairing force to 1S_0 neutron-matter gap.

N. Chamel,¹ S. Goriely,¹ and J.M. Pearson²

¹*Institut d'Astronomie et d'Astrophysique, CP-226,
Université Libre de Bruxelles, 1050 Brussels, Belgium*

²*Dépt. de Physique, Université de Montréal,
Montréal (Québec), H3C 3J7 Canada*

(Dated: October 29, 2018)

Abstract

In this latest of our series of Skyrme-HFB mass models, HFB-16, we introduce the new feature of requiring that the contact pairing force reproduce at each density the 1S_0 pairing gap of neutron matter as determined in microscopic calculations with realistic nucleon-nucleon forces. We retain the earlier constraints on the Skyrme force of reproducing the energy-density curve of neutron matter, and of having an isoscalar effective mass of $0.8M$ in symmetric infinite nuclear matter at the saturation density; we also keep the recently adopted device of dropping Coulomb exchange. Furthermore, the correction term for the spurious energy of collective motion has a form that is known to favour fission barriers that are in good agreement with experiment. Despite the extra constraints on the effective force, we have achieved a better fit to the mass data than any other mean field model, the rms error on the 2149 measured masses of nuclei with N and $Z \geq 8$ having been reduced to 0.632 MeV; the improvement is particularly striking for the most neutron-rich nuclei. Moreover, it turns out that even with no flexibility at all remaining for the pairing force, the spectral pairing gaps that we find suggest that level densities in good agreement with experiment should be obtained. This new force is thus particularly well-suited for astrophysical applications, such as stellar nucleosynthesis and neutron-star crusts.

PACS numbers: 21.10.Dr, 21.30.-x, 21.60.Jz, 26.60.Gj

I. INTRODUCTION

The r-process of stellar nucleosynthesis is known to depend on the masses and fission barriers (among other quantities) of nuclei that are so neutron-rich that there is no hope of being able to measure them in the laboratory in the foreseeable future [1]. Moreover, the composition of the outer crust of neutron stars depends on the masses of nuclei lying as far out on the nuclear chart as the neutron drip line [2]. It is thus of the greatest importance to be able to make reliable extrapolations of these quantities away from the known region, relatively close to the stability line, out towards the neutron drip line. In order to put these extrapolations on as rigorous a footing as is feasible at the present time we have constructed a series of mass models based on the Hartree-Fock-Bogoliubov (HFB) method with Skyrme forces and a contact pairing force [3, 4, 5, 6, 7, 8, 9, 10, 11], the parameters of which are fitted to essentially all the available mass data. Clearly, the fit to the mass data must be as good as possible; hitherto our best fit was that of model HFB-8 [7], for which the rms deviation with respect to the 2149 measured masses of nuclei with N and $Z \geq 8$ given in the most recent data compilation, the 2003 Atomic Mass Evaluation (AME) [12], is 0.635 MeV.

However, masses are not the only nuclear quantity of astrophysical interest that can be calculated with an effective interaction, and we have been paying an increasing amount of attention to such questions as level densities, fission barriers and various properties of the inner crust of neutron stars (see Section 5 of Ref. [8] for a brief discussion of the structure of neutron stars that is sufficient for our present purposes, and Refs. [2] for a more complete account). Our ultimate aim is to construct a universal nuclear effective interaction for all the various astrophysical applications, and to this end we have been imposing on our mass models an increasing number of relevant constraints, even if this entails a slight deterioration in the quality of the mass fit. The progress made so far in this respect can be summarized as follows.

i) To make reliable calculations of the inner crust of neutron stars, where neutron-rich clusters coexist with a neutron liquid which may be superfluid, it is essential that the value of the effective mass implied by the effective interaction be realistic. For its isoscalar component M_s^* the preferred value at the equilibrium density ρ_0 of symmetric infinite nuclear matter (INM) is around $0.8M$ (see Ref. [10] for a summary of the experimental and theo-

retical evidence). While a phenomenological value of M_s^*/M much closer to unity had been traditionally regarded as essential for good masses in mean-field calculations, we showed [6] that it is possible to have fits that are almost as good with M_s^*/M taking the realistic value of 0.8. The key to this success lay with exploiting the degree of freedom associated with the pairing ; it should nevertheless be stressed that reducing M_s^*/M in this way still has an adverse effect on single-particle (s.p.) spectra in the vicinity of the Fermi level [6].

ii) Beginning with mass model HFB-9 [8] we require that the effective interaction reproduce the energy-density curve of neutron matter, as calculated with realistic 2- and 3-nucleon forces [13]. Not only is this condition obviously relevant to all neutron-star applications, but it will also improve confidence in finite-nucleus extrapolations out towards the neutron drip line. Of all our constraints this was the one having the most adverse effect on the mass fit, but it was still possible to hold the deterioration to within tolerable limits.

iii) By taking a pairing force that was weaker than that of model HFB-9 and of all earlier models we found that it was possible, for the first time with our models, to obtain level densities in reasonable agreement with experiment [9, 14], while maintaining an acceptable mass fit.

iv) By making a phenomenological adjustment of the collective correction it is possible to fit both masses and fission barriers within the same model (HFB-14) [10].

v) Our latest model (HFB-15) [11] incorporates the frequently recommended procedure of dropping Coulomb exchange, thereby simulating neglected effects such as Coulomb correlations, charge-symmetry breaking of the nuclear forces, vacuum polarization, etc. A significant improvement in the mass-data fit was achieved.

As an alternative to non-relativistic Skyrme-based mass models, mass models based on the relativistic mean-field (RMF) method have also been proposed [15, 16]. Now the isospin dependence of the spin-orbit field is *formally* quite different in the two approaches, and it might be thought that RMF models would provide more reliable extrapolations to the neutron drip line, since one must inevitably prefer a model that respects Lorentz covariance to one that does not, other things being equal. However, it has been shown that if the same mass data are fitted equally well in the two approaches then essentially the same predictions are made out at the neutron drip line [17]. Thus we believe that the Skyrme approach is just as reliable as the RMF method; in any case, the latter method has not yet been developed to the point where its mass fits are as good as those given by Skyrme-based methods.

In the present paper we impose the additional constraint force of requiring that the effective interaction reproduce as a function of density the microscopic 1S_0 pairing gap of neutron matter, while retaining all the constraints of the earlier papers. Without this new constraint it would be impossible to make reliable investigations of a possible superfluid phase in the inner crust of neutron stars. For this purpose, we develop a scheme first proposed by Duguet [18] for constructing an effective density-dependent contact pairing interaction which reproduces *any* given microscopic gap *exactly*. Instead of parametrizing the density dependence by a simple functional form, the strength of the contact interaction is determined at each density by solving directly the HFB equations in neutron matter, and requiring that the resulting gap be equal to the given microscopic gap at the Fermi momentum corresponding to that density.

In Section II we describe the way in which we implement the HFB method, with particular emphasis on points that we overlooked in our earlier description in Ref. [3]. Section III explains our procedure for determining the strength of the pairing force, while the results of the new mass fit are presented in Section IV. The two appendices summarize some relevant features of the HFB method.

II. THE HFB METHOD

The Skyrme force that we use in the present calculations has, as with all our previous HFB mass models, the conventional form

$$\begin{aligned} v^{\text{Sky}}(\mathbf{r}_i, \mathbf{r}_j) = & t_0(1 + x_0 P_\sigma) \delta(\mathbf{r}_{ij}) + \frac{1}{2} t_1(1 + x_1 P_\sigma) \frac{1}{\hbar^2} [p_{ij}^2 \delta(\mathbf{r}_{ij}) + \delta(\mathbf{r}_{ij}) p_{ij}^2] \\ & + t_2(1 + x_2 P_\sigma) \frac{1}{\hbar^2} \mathbf{p}_{ij} \cdot \delta(\mathbf{r}_{ij}) \mathbf{p}_{ij} + \frac{1}{6} t_3(1 + x_3 P_\sigma) \rho(\mathbf{r})^\gamma \delta(\mathbf{r}_{ij}) \\ & + \frac{i}{\hbar^2} W_0(\boldsymbol{\sigma}_i + \boldsymbol{\sigma}_j) \cdot \mathbf{p}_{ij} \times \delta(\mathbf{r}_{ij}) \mathbf{p}_{ij} \quad , \end{aligned} \quad (2.1)$$

where $\mathbf{r}_{ij} = \mathbf{r}_i - \mathbf{r}_j$, $\mathbf{r} = (\mathbf{r}_i + \mathbf{r}_j)/2$, $\mathbf{p}_{ij} = -i\hbar(\nabla_i - \nabla_j)/2$ is the relative momentum, and P_σ is the two-body spin-exchange operator. The contact pairing force that we take here acts, as before, only between nucleons of the same charge state q ($q = n$ or p for neutron or proton, respectively)

$$v_q^{\text{pair}}(\mathbf{r}_i, \mathbf{r}_j) = v^{\pi q}[\rho_n(\mathbf{r}), \rho_p(\mathbf{r})] \delta(\mathbf{r}_{ij}) \quad , \quad (2.2)$$

where $v^{\pi q}[\rho_n, \rho_p]$ is a functional of the nucleon densities that will be specified in Section III.

The only paper in which we attempt to describe the way in which we implement the HFB method is Ref. [3] (Section 2). Since this account was somewhat incomplete, and in a sense misleading, we present here a more detailed description of what we actually did. Our original presentation [3] was developed within the framework of the standard formulation of Mang [19] and of Ring and Schuck [20], which is certainly well adapted to the use of a discrete basis such as an oscillator basis, as in the case of our own calculations. Nevertheless, some clarification is necessary when this formalism is applied to effective forces of the form given in Eqs. (2.1) and (2.2).

The standard formulation [19, 20] assumes two-body forces, and starts with the expression

$$H = \sum_{ij} t_{ij} c_i^\dagger c_j + \frac{1}{4} \sum_{ij,kl} \bar{v}_{ij,kl} c_i^\dagger c_j^\dagger c_l c_k \quad (2.3)$$

for the Hamiltonian (see, for example, Eq. (5.25) of Ref. [20]). Here we are working in a fixed basis of discrete s.p. states labelled by i, j , etc., e.g., an oscillator basis, with $c_i^\dagger(c_j)$ denoting creation (destruction) operators for real nucleons in such states (the charge type is implicit in the label). Also we have introduced the antisymmetrized matrix element of the two-body force

$$\bar{v}_{ij,kl} = v_{ij,kl} - v_{ij,lk} \quad , \quad (2.4)$$

and the matrix element t_{ij} of the kinetic-energy operator $-\hbar^2 \nabla^2 / 2M_q$, denoting the nucleon mass by M_q .

The Bogoliubov transformation

$$\begin{aligned} \beta_k^\dagger &= \sum_l (U_{lk} c_l^\dagger + V_{lk} c_l) \\ \beta_k &= \sum_l (U_{lk}^* c_l + V_{lk}^* c_l^\dagger) \end{aligned} \quad (2.5)$$

then defines creation (destruction) operators $\beta_k^\dagger(\beta_k)$ of quasiparticles as linear combinations of the creation and destruction operators of real nucleons. The essence of the HFB method is that it takes the vacuum state of these quasiparticles as the trial function for a variational approximation to the energy of the nucleus. Denoting this (normalised) vacuum state by $|\Psi\rangle$, and noting that it will be a function of the transformation coefficients U_{lk}, V_{ij} , etc., the HFB ground-state energy becomes, as for example in Eq. (E.20) of Ref. [20],

$$E_{\text{HFB}} \equiv \langle \Psi | H | \Psi \rangle = \text{Tr} \left(t\rho + \frac{1}{2} \Gamma \rho - \frac{1}{2} \Delta \kappa^* \right) \quad , \quad (2.6)$$

in which Tr denotes the trace, ρ and κ are the so-called normal and abnormal density matrices, respectively,

$$\rho_{ij} = \langle \Psi | c_j^\dagger c_i | \Psi \rangle = \sum_l V_{il}^* V_{jl} = \rho_{ji}^* \quad (2.7a)$$

and

$$\kappa_{ij} = \langle \Psi | c_j c_i | \Psi \rangle = \sum_l V_{il}^* U_{jl} = -\kappa_{ji} \quad , \quad (2.7b)$$

while

$$\Gamma_{kl} = \sum_{ij} \bar{v}_{ki,lj} \rho_{ji} \quad (2.8a)$$

and

$$\Delta_{kl} = \frac{1}{2} \sum_{ij} \bar{v}_{kl,ij} \kappa_{ij} \quad . \quad (2.8b)$$

We now notice the first departure from this standard formulation that we have to make on account of our choice of effective forces of the form given in Eqs. (2.1) and (2.2). Although Eq. (2.6) remains valid, along with Eqs. (2.4), (2.5), (2.7a) and (2.7b), because the force in the particle-particle channel is different from the one used in the particle-hole channel we must replace Eqs. (2.8a) and (2.8b), respectively, by

$$\Gamma_{kl} = \sum_{ij} \bar{v}_{ki,lj}^{\text{Sky}} \rho_{ji} + \sum_{ij} \bar{v}_{ki,lj}^{\text{Coul}} \rho_{ji} \quad , \quad (2.9a)$$

where $\bar{v}_{ki,lj}^{\text{Coul}}$ are the antisymmetrized matrix elements of the Coulomb interaction, and

$$\Delta_{kl} = \frac{1}{2} \sum_{ij} \bar{v}_{kl,ij}^{\text{pair}} \kappa_{ij} \quad , \quad (2.9b)$$

in which the choice of force in the respective channels is made explicit. This distinction was made clear in our first HFB paper [3] (see Eq. (7) of that paper, where, however, there was an error in the subscripts of the expression for Γ_{kp}), but it was incorrect to imply that we could still take a Hamiltonian of the form (2.3) as the starting point: this would be possible only if no matrix element $\bar{v}_{ki,lj}$ appeared in both Γ_{kl} and Δ_{kl} , which is not the case. Rather, one should really proceed via a density-functional approach, as discussed below.

The second departure from the standard formulation that we are obliged to make because of our choice of effective forces was not made clear at all in Ref. [3]. The HFB equations resulting from the minimization of the total ground-state energy (2.6) are

$$\sum_j \begin{pmatrix} h'_{ij} - \lambda \delta_{ij} & \Delta_{ij} \\ -\Delta_{ij}^* & -h'_{ij} + \lambda \delta_{ij} \end{pmatrix} \begin{pmatrix} U_{jk} \\ V_{jk} \end{pmatrix} = E_k \begin{pmatrix} U_{ik} \\ V_{ik} \end{pmatrix}, \quad (2.10)$$

where E are the quasi-particle energies, and λ is the usual chemical potential, arising as a Lagrange multiplier. Also

$$h'_{ij} = \frac{\partial E_{\text{HFB}}}{\partial \rho_{ji}} = h_{ji}^*, \quad (2.11a)$$

denoting matrix elements of the self-consistent s.p. Hamiltonian, and

$$\Delta_{ij} = \frac{\partial E_{\text{HFB}}}{\partial \kappa_{ij}^*} = -\Delta_{ji}, \quad (2.11b)$$

denoting matrix elements of the pairing potential. Now Eq. (2.10) differs from Eq. (6) of Ref. [3] in that the quantity h_{ij} defined in the first member of Eq. (7) of that paper,

$$h_{ij} = t_{ij} + \Gamma_{ij}, \quad (2.12)$$

has been replaced here by

$$h'_{ij} = h_{ij} + h_{ij}^{\text{rear}}, \quad (2.13)$$

where we have introduced matrix elements of the rearrangement s.p. field

$$h_{ij}^{\text{rear}} \equiv \frac{1}{2} \sum_{klpm} \left(\frac{\partial \bar{v}_{kl,pm}^{\text{Sky}}}{\partial \rho_{ji}} \rho_{ml} \rho_{pk} - \frac{1}{2} \frac{\partial \bar{v}_{kl,pm}^{\text{pair}}}{\partial \rho_{ji}} \kappa_{pm} \kappa_{lk}^* \right), \quad (2.14)$$

which arises entirely from the derivative with respect to density of the density-dependent components of the force (the Coulomb interaction is independent of the density and therefore does not lead to rearrangement terms). Although these rearrangement terms were omitted from Eq. (6) of Ref. [3], they were included in all our actual calculations. (The rearrangement terms were also dropped from Eq. (7.42) of Ref. [20], and from Eq. (14) of Ref. [58]. Note also that Eq. (7.42) of Ref. [20] absorbs λ into h .) Let us remark that the forces considered in this work depend only on the normal nucleon densities but not on the abnormal densities, whence the expressions (2.11b) and (2.9b) are equivalent. The foregoing formalism could

certainly be implemented if one calculated the two-body matrix elements $\bar{v}_{ij,kl}^{\text{Sky}}$ and $\bar{v}_{ij,kl}^{\text{pair}}$ for forces (2.1) and (2.2), respectively, in the oscillator basis. However, although this presents no problem of principle, it is not what one does, despite suggestions to the contrary in Ref. [3]. Rather, one follows a simpler approach that does not require the calculation of these matrix elements, even if one still solves the HFB equations (2.10) in the oscillator basis, as we do here. Instead of starting with the Hamiltonian (2.3), one begins by noting that for zero-range interactions, such as forces (2.1) and (2.2) considered in this work, the HFB energy can be written as the integral of a purely local energy-density functional

$$E_{\text{HFB}} = \int \mathcal{E}_{\text{HFB}}(\mathbf{r}) d^3\mathbf{r} \quad , \quad (2.15)$$

where, assuming time reversibility, as always in this paper,

$$\begin{aligned} \mathcal{E}_{\text{HFB}}(\mathbf{r}) = & \mathcal{E}_{\text{Sky}} \left[\rho_n(\mathbf{r}), \nabla \rho_n(\mathbf{r}), \tau_n(\mathbf{r}), \mathbf{J}_n(\mathbf{r}), \rho_p(\mathbf{r}), \nabla \rho_p(\mathbf{r}), \tau_p(\mathbf{r}), \mathbf{J}_p(\mathbf{r}) \right] \\ & + \mathcal{E}_{\text{Coul}} \left[\rho_p(\mathbf{r}) \right] + \mathcal{E}_{\text{pair}} \left[\rho_n(\mathbf{r}), \tilde{\rho}_n(\mathbf{r}), \rho_p(\mathbf{r}), \tilde{\rho}_p(\mathbf{r}) \right] \quad , \end{aligned} \quad (2.16)$$

in which the usual normal density ρ_q , kinetic-energy density τ_q , spin-current density \mathbf{J}_q and pairing density $\tilde{\rho}_q$ appear (see Appendix A for precise definitions).

Expressions for the first term in Eq. (2.16), the energy density associated with the Skyrme force (2.1) and implicitly including the kinetic energy, can be found, for example, in Ref. [21]. The second term in Eq. (2.16) represents the Coulomb-energy density, the exchange part of which is treated in our code by the Kohn-Sham approximation [22] (usually referred to as the Slater approximation in the nuclear-physics literature, but the original Slater version [23] is somewhat different), assuring thereby that the energy-density functional remains local. Actually, in the model described in the present paper, HFB-16, we drop the Coulomb-exchange term, as discussed in Section I, and thus write

$$\mathcal{E}_{\text{Coul}} = \frac{1}{2} e \rho_{\text{ch}} V^{\text{Coul}} \quad , \quad (2.17)$$

in which $e \rho_{\text{ch}}$ is the charge density associated with protons (this differs from $e \rho_p$ because we are taking account of the finite size of the proton), and V^{Coul} is the electrostatic potential, given by

$$V^{\text{Coul}}(\mathbf{r}) = e \int d^3\mathbf{r}' \frac{\rho_{\text{ch}}(\mathbf{r}')}{|\mathbf{r} - \mathbf{r}'|} \quad . \quad (2.18)$$

The last term in Eq. (2.16) is the pairing-energy density, associated with the pairing force (2.2), and is given by

$$\mathcal{E}_{\text{pair}}(\mathbf{r}) = \frac{1}{4} \sum_{q=n,p} v^{\pi q} [\rho_n(\mathbf{r}), \rho_p(\mathbf{r})] \tilde{\rho}_q(\mathbf{r})^2. \quad (2.19)$$

By taking a density functional of the general form given by Eqs. (2.16), rather than the Hamiltonian (2.3), as the starting point, the possibility of having different equivalent forces in the particle-hole and particle-particle channels arises quite naturally. Indeed, in this formulation the forces never have to appear explicitly, and one even has the freedom to choose the form of the functional in such a way that no corresponding forces exist at all. However, in this paper our choice of functional does correspond rigorously to forces of the form (2.1) and (2.2), as we have already indicated.

When the HFB energy is expressed in terms of an energy-density functional, as in Eqs. (2.15) and (2.16), then minimizing it with respect to the normal and pairing density matrices, for a fixed average number of neutrons and protons, leads to the HFB equations in coordinate space, as shown by Dobaczewski and co-workers [24, 25] (the link with the discrete-basis formulation (2.10) is discussed at the end of Appendix A). The advantage of solving the HFB equations in coordinate space, as in Refs. [24, 25], is that it facilitates an accurate determination of the asymptotic wavefunctions, but it has little impact on the determination of binding energies, which are our main concern. Thus for convenience we solve the HFB equations in the discrete-basis form (2.10). An essential step in this solution is the computation of the oscillator matrix elements (2.11a) and (2.11b), but we considerably simplify the numerical task by generalizing to HFB the procedure outlined by Vautherin for the first HF-BCS calculation of deformed nuclei [26]. This procedure (see Appendix A for more details) works essentially in an oscillator basis but makes a detour into the coordinate-space representation by expressing these matrix elements as matrix elements of the self-consistent s.p Hamiltonian $h'_q(\mathbf{r})_{\sigma'\sigma}$ and the self-consistent pairing field $\Delta_q(\mathbf{r})$, respectively, both of which appear in the coordinate-space form of the HFB equations (A.18), (explicit expressions for both these fields are given in Appendix A). In this way the computation of the far more numerous matrix elements (2.4) of the two-body force is no longer required. From this point on, our calculations proceed on the general lines described in Ref. [3].

III. DETERMINATION OF DENSITY DEPENDENCE OF PAIRING FORCE

Little is known about the density dependence of the effective pairing interaction. The simplest ansatz, commonly referred to as “volume pairing”, is simply to assume that $v^{\pi q}[\rho_n, \rho_p] = V^{\pi q}$, a constant, independent of the density, in which case the corresponding rearrangement term vanishes. This prescription has been adopted for all our previous forces except for the parameter sets BSk3 [5], BSk5 [6] and BSk7 [6], for which we considered a density dependence of the usual form

$$v^{\pi q}[\rho_n, \rho_p] = V_{\pi q} \left\{ 1 - \eta \left(\frac{\rho}{\rho_0} \right)^\alpha \right\} \quad , \quad (3.1)$$

where $\rho = \rho_n + \rho_p$, while $V_{\pi q}$, η and α are adjustable parameters. Testing different sets of parameters, it was concluded that this particular form (3.1) does not improve the global fit to the experimental mass data, and we thus abandoned it in our subsequent parametrizations. However, if one is to reproduce not only masses but also the microscopic pairing gaps given by bare nucleon-nucleon potentials, i.e., interactions fitted directly to the 2- and 3-nucleon data, then the effective pairing force must be density dependent, as was first shown by Garrido *et al.* [27] with a contact pairing force with the functional form (3.1).

In the present paper, we wish to constrain our effective force to the pairing properties of pure neutron matter. Several microscopic many-body calculations of the 1S_0 pairing gaps have been carried out using various approaches and approximation schemes. Calculations at the simplest BCS level with the free s.p. spectrum for different nucleon-nucleon potentials yield very similar results [28, 29, 30]. In fact, at this level the pairing gap is essentially determined by the experimental 1S_0 phase shifts [31]. Calculations going beyond the BCS approximation generally show that medium effects lower the maximum of the gap function $\Delta_n(\rho_n)$ but they disagree among themselves as to the precise density dependence. (Note that we use the notation $\Delta_n(\rho_n)$ for the pairing gap evaluated at the Fermi momentum $k_{Fn} = (3\pi^2\rho_n)^{1/3}$.) Given this lack of agreement, we take here for the microscopic pairing gap the one shown in Fig. 7 of Ref. [28], given by the realistic Argonne v_{14} force in the BCS approximation. In any case, recent quantum Monte-Carlo calculations [32, 33, 34, 35] suggest that the “true” gap might be actually close to the BCS one.

We show this microscopic BCS gap as a function of neutron-matter density in Fig. 1; for

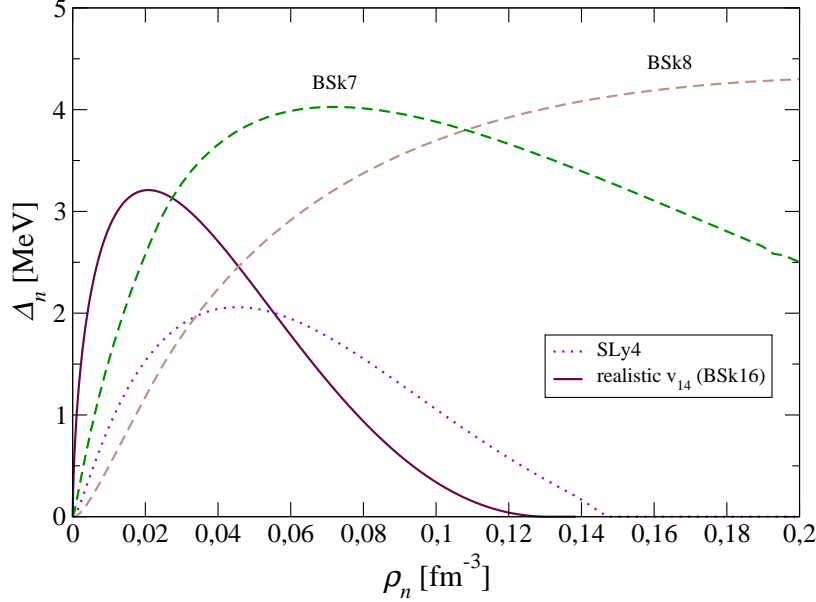


FIG. 1: 1S_0 pairing gap Δ_n of neutron matter as a function of the density ρ_n calculated at the Fermi momentum $k_{Fn} = (3\pi^2\rho_n)^{1/3}$ for the realistic Argonne v_{14} interaction [28], and various effective forces. Note that the effective force BSk16 derived in this paper yields a pairing gap indistinguishable from the curve labelled “realistic v_{14} (BSk16)”.

convenience, we have used the essentially exact analytical representation [36]

$$\Delta_n(\rho_n) = \theta(k_{\max} - k_{Fn}) \Delta_0 \frac{k_{Fn}^2}{k_{Fn}^2 + k_1^2} \frac{(k_{Fn} - k_2)^2}{(k_{Fn} - k_2)^2 + k_3^2}, \quad (3.2)$$

where θ is the Heaviside unit-step function, and the associated parameters are given in Table I. For comparison, we also display in the same figure the gaps corresponding to various effective interactions. The large differences between the neutron matter gaps for our forces BSk7 and BSk8 is particularly striking, given that they both yield good mass fits and hence comparable pairing gaps in finite nuclei. The gap obtained with the force BSk7 is closer to the microscopic one, which might be related to the fact that its pairing component is density dependent, but the discrepancy with respect to the microscopic gap is still quite unacceptable. Much better agreement is found for the Skyrme force SLy4 [37], using the pairing adopted in Ref.[38]. However, the rms deviation of the mass fit given by this model is very large (5.1 MeV for the subset of even-even nuclei [38, 39]). In the present paper we show that despite the failure of the BSk7 and BSk8 models to yield acceptable pairing gaps in neutron matter, it is still possible to construct a modified BSk model that fits the microscopic pairing gap of neutron matter *exactly*, while maintaining the quality of the mass

fits obtained with our earlier models. We label the new model BSk16, as indicated in Fig. 1.

Now if we adopted the parametrization (3.1) for the density dependence of the contact pairing force in our new mass model a serious problem would arise. In any calculation of this sort the values of the pairing parameters depend on the effective interaction adopted in the particle-hole channel, essentially through the effective mass (see Eqns. (3.3) and (3.4) below). In the case of the work of Garrido *et al.* [27], a specific force (Gogny) was chosen at the outset as the interaction for the particle-hole channel, whence the parameters $V_{\pi q}$, η and α of the pairing force (3.1) could be easily fitted to a microscopic pairing gap. However in the present work, the parameters of the Skyrme force acting in the particle-hole channel are not known *a priori* but rather are determined *a posteriori* by fitting to experimental nuclear mass data, as discussed in Section IV. Fitting the parameters of the effective interaction in both the particle-hole and particle-particle channels, while simultaneously reproducing the microscopic pairing gap $\Delta_q(\rho_q)$, would be an extremely onerous numerical task when using a phenomenological functional, such as Eq. (3.1). Moreover, there is no guarantee that the parametrization (3.1) of the density dependence will be optimal in general, as indicated in Ref. [40], even though it works well in the case considered by Garrido *et al.* [27]. Both of the above problems are avoided in the fitting procedure that we adopted in the present paper, and now describe.

Following Duguet [18] and more recent calculations [41], we assume that the pairing force for nucleons q depends only on ρ_q , and not on the total density ρ . Besides, we suppose that the effective interaction $v^{\pi q}[\rho_q(\mathbf{r})]$ at the point \mathbf{r} is the same as that in INM of pure nucleon species q at the density $\rho_q(\mathbf{r})$. But instead of postulating a simple functional form for the density dependence, we have determined the strength of the effective pairing force $v^{\pi q}[\rho_q]$ at each nucleon density ρ_q by solving the HFB equations in uniform matter and requiring that the resulting gap reproduce *exactly* the given microscopic pairing gap $\Delta_q(\rho_q)$ at that density. The only free parameter is the energy cutoff ε_Λ . Note that in the present work, we have set an upper limit on the s.p. states that are retained in the spectrum without using the Bulgac-Yu [42] regularization procedure, which we adopted in models HFB-12 to HFB-15 [9, 10, 11].

In uniform matter, the HFB equations reduce to the BCS equations (B.8) and (B.9). Solving these equations for $v^{\pi q}[\rho_q]$ in pure matter of nucleon species q and adopting the cutoff prescription (iii) discussed in Appendix B, yields (after a change of variable $\xi = \varepsilon - U_q$

in the integrals)

$$v^{\pi q}[\rho_q] = -8\pi^2 \left(\frac{\hbar^2}{2M_q^*(\rho_q)} \right)^{3/2} \left(\int_0^{\mu_q + \varepsilon_\Lambda} d\xi \frac{\sqrt{\xi}}{\sqrt{(\xi - \mu_q)^2 + \Delta_q(\rho_q)^2}} \right)^{-1}, \quad (3.3)$$

where $M_q^*(\rho_q)$ is the effective nucleon mass in matter of pure nucleon species q at density ρ_q , as given by Eq. (A.14), and $\mu_q \equiv \lambda_q - U_q$ can be obtained by solving

$$\rho_q = \frac{1}{4\pi^2} \left(\frac{2M_q^*(\rho_q)}{\hbar^2} \right)^{3/2} \int_0^\infty d\xi \sqrt{\xi} \left(1 - \frac{\xi - \mu_q}{\sqrt{(\xi - \mu_q)^2 + \Delta_q(\rho_q)^2}} \right). \quad (3.4)$$

Note that determining the strength $v^{\pi q}$ of the effective pairing force by Eq. (3.3) ensures its automatic renormalization for any changes of the energy cutoff ε_Λ . The same value of ε_Λ is used in calculations of finite nuclei (see Eq. (4.3) below). Let us remark that if, instead of imposing a cutoff above the Fermi level, we would have chosen a fixed cutoff (as was done in model HFB-1 [3]), Eq. (3.3) would have been actually an integro-differential equation for $v^{\pi q}[\rho_q]$ as discussed in Appendix B. In such case, it would therefore have been much more difficult to compute the strength of the effective pairing force.

In contrast to the use of parametrized pairing forces (3.1), in the present scheme we reproduce *exactly* the density dependence of the microscopic pairing gap. At the same time, the fitting procedure of the Skyrme parameters is greatly simplified: at each iteration of the mass fit, the pairing function $v^{\pi q}[\rho_q]$ is determined unambiguously through the coupled equations (3.3) and (3.4) by the given microscopic gap $\Delta_n(\rho_n)$ and the running values of the Skyrme parameters t_1 , t_2 , x_1 and x_2 .

In our actual numerical calculations, instead of solving both Eqs. (3.3) and (3.4) at each density, we approximate the reduced chemical potential μ_q by the Fermi energy

$$\varepsilon_F^{(q)} = \frac{\hbar^2 k_{Fq}^2}{2M_q^*}, \quad (3.5)$$

where k_{Fq} is the Fermi wave number

$$k_{Fq} = (3\pi^2 \rho_q)^{1/3}. \quad (3.6)$$

We have found that this approximation holds well, provided $\Delta_q \ll \varepsilon_F^{(q)}$. Then we do not have to solve Eq. (3.4) at all, and the evaluation of $v^{\pi q}[\rho_q]$ through Eq. (3.3) reduces to a single, simple integration. The effective pairing strength $v^{\pi q}[\rho_q]$ determined for the final

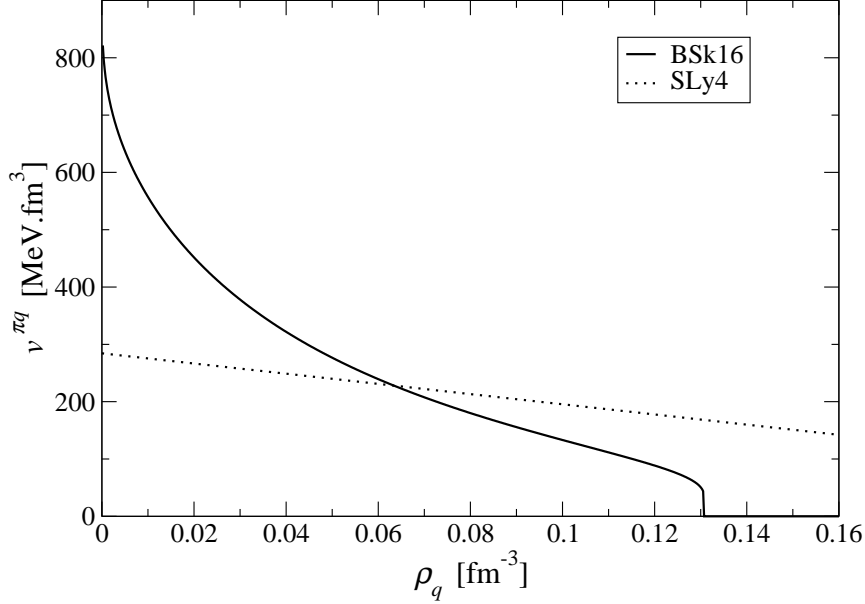


FIG. 2: Density dependence of the strength of the effective pairing force $v^{\pi q}[\rho_q]$, which has been fitted to the 1S_0 pairing gap Δ_n shown in Fig. 1. The effective mass at each density is calculated with the final BSk16 Skyrme parameters (see Section IV). For comparison, we show the effective pairing force used in the SLy4 mass model [38, 39].

Skyrme force BSk16 (see Section IV) through Eq. (3.3), is shown in Fig. 2; it will be seen that the density dependence is qualitatively similar to that given by Eq. (3.1).

The foregoing neutron-matter prescription suffices in principle to fix the neutron pairing (see, however, Section IV for the distinction that we make between even- N and odd- N nuclei). Because of charge-symmetry breaking, the proton pairing force should in principle be determined in an analogous way on the basis of “proton-matter” calculations, which are performed in exactly the same way as are neutron-matter calculations, using the appropriate proton-proton interaction, with, of course, the Coulomb force suppressed, since “proton-matter” calculations would otherwise diverge. However, this prescription will not suffice, since in finite nuclei the Coulomb force *does* act, and may be expected to modify the proton pairing, in a highly complicated way. For simplicity, we take $v^{\pi p}[\rho_p]$ to be given by $v^{\pi n}[\rho_p]$, multiplied by a constant, density-independent factor which is the same for all nuclei and is taken as a fitting parameter (see Section IV for more details).

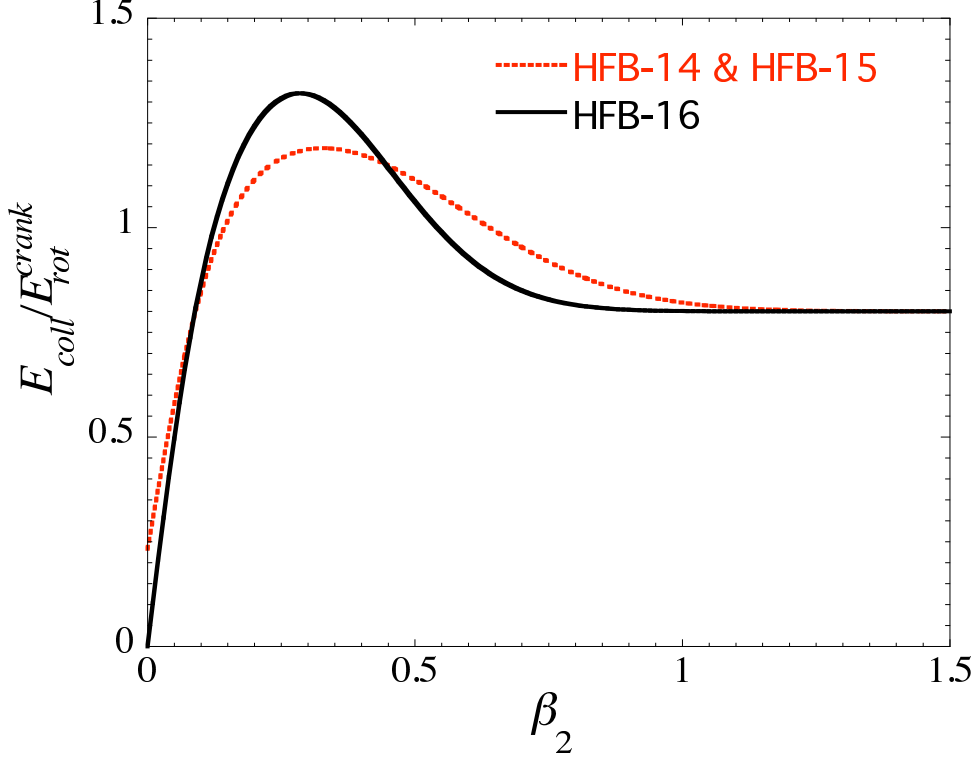


FIG. 3: Deformational variation of collective correction of Eq. (4.2).

IV. THE MASS FITS

We have described our treatment of the Skyrme and pairing forces of our new model, HFB-16, in Sections II and III, respectively, but, before presenting the parameter sets for these forces that emerge from the fits to the mass data, we discuss several further points, as follows.

i) *Wigner correction.* To the HFB energy calculated for the Skyrme force (2.1) and the pairing force (2.2) has to be added the Wigner correction

$$E_W = V_W \exp \left\{ -\lambda \left(\frac{N-Z}{A} \right)^2 \right\} + V'_W |N-Z| \exp \left\{ -\left(\frac{A}{A_0} \right)^2 \right\} , \quad (4.1)$$

which contributes significantly only for light nuclei [4]. Our treatment of this correction is purely phenomenological, with the first term believed to be representing a $T = 0$ $n - p$ pairing [43, 44, 45], while the second is characteristic of Wigner's supermultiplet theory [46], based on $SU(4)$ spin-isospin symmetry, although it can also be interpreted as corresponding to $T = 1$ $n - p$ pairing [43].

ii) *Collective correction.* As in all our previous models we subtract from the calculated

HFB energy an estimate for the spurious collective energy. The form we adopt here for this correction is

$$E_{coll} = E_{rot}^{crank} \left\{ b \tanh(c|\beta_2|) + d|\beta_2| \exp\{-l(|\beta_2| - \beta_2^0)^2\} \right\} , \quad (4.2)$$

in which E_{rot}^{crank} denotes the cranking-model value of the rotational correction and β_2 the quadrupole deformation, while all other parameters are free fitting parameters. This correction is intended to take account of both rotational and vibrational spurious energy, but while this expression for E_{coll} is seen to vanish for spherical nuclei, we know that a vibrational correction is still required for such nuclei. Thus we must suppose that the vibrational correction for spherical nuclei is absorbed into the fitted force parameters, so that it is only the deformational variation of the vibrational correction that is represented by Eq. (4.2), along with the complete rotational correction. Our final mass fit gives for the coefficient b appearing in the first term of Eq. (4.2) the value of 0.8 (see Table III), the same value as we found for model HFB-14 [10]. Thus the argument that was made in Ref. [10] points once again to the first term of Eq. (4.2) being identified with the rotational correction.

Actually, the second term of the correction (4.2) differs from that of model HFB-14 [10] in that it carries an additional factor $|\beta_2|$, the role of which is to ensure that this term, like the first term, vanishes as sphericity is approached. Some instabilities that were encountered for spherical or weakly deformed nuclei with HFB-14 [10] are thereby avoided, and this modification is in part responsible for the improved mass fit of this new model (see below in this Section). The corrections for the two models are compared graphically in Fig. 3, where it will be seen that except in the spherical limit the differences between the two corrections are small, especially for large deformations. This point is of crucial importance for fission barriers, which are highly sensitive to the collective correction at large deformations, and we do not expect that the barriers to be calculated (in a future paper) with the present model will be appreciably different from those found with model HFB-14. In any case, it will be possible to perform any fine tuning of the barriers that may be required by adjustment of the collective correction alone, without any modification of the Skyrme or pairing parameters, our experience in Ref. [10] showing that the perturbation of the mass fit will be minimal, provided the collective contribution has the form (4.2).

iii) As with models HFB-14 [10] and HFB-15 [11], we impose on the parameters of the Skyrme force the condition $M_s^*/M = 0.8$ for the isoscalar effective mass in symmetric INM

at the density $\rho = \rho_0$ (see Section I).

iv) By varying the exponent γ the incompressibility coefficient K_v can be varied, and we find that excellent mass fits can be obtained over the range $230 \leq K_v \leq 270$ MeV. However, measurements of the breathing mode restrict this range to $230 \leq K_v \leq 250$ MeV [47, 48], so we limit the value of γ accordingly.

v) The measured rms charge radius R_c of ^{208}Pb , 5.501 ± 0.001 fm [49], was required to be well reproduced; relaxing this condition leads to very little improvement in the mass fit.

vi) As with all our models since HFB-9 [8], we constrain our Skyrme force to fit neutron matter (see Section I); this turns out to be equivalent to setting the INM parameter J to be 30 MeV.

vii) We drop the Coulomb-exchange term from the HFB energy-density functional (see Section I).

viii) As with all our models, we treat the case of odd N and/or odd Z by the “level-filling” approximation. That is, the odd nucleon is placed with equal probability in each of the lowest-energy available degenerate states generated by the HF calculation with the next lowest even number of nucleons, and then applying blocking.

ix) Our new prescription for the pairing strength, described in Section III, is strictly valid only for neutrons. Because of Coulomb effects, and a possible charge-symmetry breaking of nuclear forces, we must allow for the proton pairing strength to be different. Likewise, we shall allow the pairing to be different for odd- A and odd-odd nuclei to compensate for our failure for such nuclei to project out states that respect time-reversal invariance. We take account of these extra degrees of freedom by multiplying the value of $v^{\pi q}[\rho_q]$, as determined through Eq. (3.3), by renormalizing factors f_q^\pm , where f_p^+ , f_p^- and f_n^- are free, density-independent parameters to be included in the mass fit; in keeping with the spirit of this paper we set $f_n^+ = 1$.

x) In calculations of finite nuclei, we use the smooth pairing cutoff factor

$$f_i = \left[1 + \exp((\varepsilon_i - \lambda - \varepsilon_\Lambda)/\tau) \right]^{-1/2} \quad (4.3)$$

with $\tau = 0.25$ MeV, in order to prevent an unphysical selection of nearly degenerate levels whenever the cutoff energy lies between the levels.

xi) The spurious centre-of-mass energy is removed following the essentially exact procedure described in Ref. [6].

xii) A correction for the finite size of the proton is made to both the charge radius and the energy, as in all our previous HFB models. We assume a Gauss distribution of charge over the proton, with an rms radius of 0.895 fm [50]; the folding of this charge distribution over the HFB distribution of point protons is performed using Eqs. (4.2) and (4.3) of Ref. [51].

xiii) As in all our papers except Ref. [7] we make no attempt to project out states of good particle number.

xiv) The oscillator basis in terms of which the HFB wavefunctions are expanded contains 20 major shells.

The new force parameters, labelled BSk16, are fitted to the same set of 2149 measured masses [12] as are all our models since HFB-9 [8]; the resulting values are shown in Table II, while Table III shows the parameters of the collective correction of Eq. (4.2). These two tables define the HFB-16 model, with which we have constructed a complete mass table running from one drip line to the other over the range Z and $N \geq 8$ and $Z \leq 110$.

The first ten lines of Table II show the Skyrme parameters; their only noteworthy feature is the small value of t_2 and the large value of x_2 , which implies that the 1P and 3P interactions have strengths of comparable magnitude but opposite sign, the latter being attractive. The next three lines show the factors by which the pairing strength determined from neutron matter must be renormalized for protons and for odd nuclei. With $f_n^+ = 1$ we see that to within the limits of numerical accuracy $f_n^-/f_n^+ = f_p^-/f_p^+$ and the proton and neutron pairing strengths are effectively equal. This means that these three degrees of freedom could have been reduced to a single one, the ratio of the odd-number pairing strength to the even-number pairing strength (as in all our previous models, pairing is always a little stronger for an odd number of nucleons). Line 14 shows the pairing cutoff parameter ε_Λ ; the value of 16 MeV was chosen on the basis of past experience [9]. The last four lines give the Wigner parameters of Eq. (4.1).

The rms and mean (data - theory) values of the deviations between the measured masses and the HFB-16 predictions are given in the first and second lines, respectively, of Table IV, where we also compare with HFB-15 [11], HFB-14 [10] and our previous “best-fit” model HFB-8 [7]. We see that with this new model we have achieved our best fit ever ($\sigma = 0.632$ MeV), in addition to having a greater conformity to physical reality than with any of our other models. It should be recalled that the first physical constraint we imposed on our mass fits, conformity to the neutron-matter energy-density curve, led, with model HFB-9 [8], to

a serious loss in the quality of the mass fit. However, we have now entirely recovered the precision of model HFB-8; this could be a result of the device of dropping Coulomb exchange (introduced in model HFB-15 [11]), of modifying the collective correction discussed above, or of requiring a better agreement with the BCS neutron-matter pairing gap. Concerning this last point, we should emphasize that starting from a neutron-matter gap that includes medium effects beyond the BCS approximation, we were not able to obtain a good mass fit. Fitting masses to such microscopic gaps seems to be very difficult in the present framework.

The superiority of the new model becomes still more striking on looking at the next six lines of Table IV. Lines 3 and 4 show the rms and mean deviations for the astrophysically crucial subset of the mass data consisting of the 185 neutron-rich nuclei having a neutron-separation energy $S_n \leq 5.0$ MeV. The following four lines give the rms and mean deviations for the S_n and the beta-decay energies Q_β , using the full data set of 2149 measured masses: since these are differential quantities they are astrophysically more relevant than the absolute masses M . It is noteworthy that in all these important categories of mass-related quantities model HFB-16 out-performs all our other HFB models.

Turning to charge radii, lines 9 and 10 show the rms and mean deviations between the measured values [49] and the model predictions. Only here do we see any deterioration with respect to model HFB-8; the mean deviation $\bar{\epsilon}(R_c)$ suggests that from model HFB-14 onwards we should have been taking a slightly larger density ρ_0 , but we do not know whether this would have an adverse effect on the mass fit.

As stated in Section I, one of our concerns has been to have a pairing force that not only permits a good mass fit but also is consistent with level densities that are in reasonable agreement with experiment. However, in the present model the pairing force is fixed almost entirely by the *a priori* calculated pairing properties of neutron matter, the flexibility offered by the renormalization factors f_q^\pm being negligible in this respect. Now previous experience with model HFB-13 [9, 14] shows that reasonable level densities are found when the spectral pairing gap $\langle uv\Delta \rangle$ of the model (defined as in Eq. (5) of Ref. [9]) lies close to the fifth-order experimental even-odd mass differences $\Delta^{(5)}$. We compare in Fig. 4 the HFB-16 spectral pairing gaps for the Sn and Pb isotope chains with those of model HFB-13 [9]. It will be seen that the new model HFB-16 agrees closely with the earlier one in the case of the Pb isotopes, and is not substantially stronger in the case of the Sn isotopes (similar conclusions hold for the third-order even-odd differences $\Delta^{(3)}$). We leave for a later paper the actual

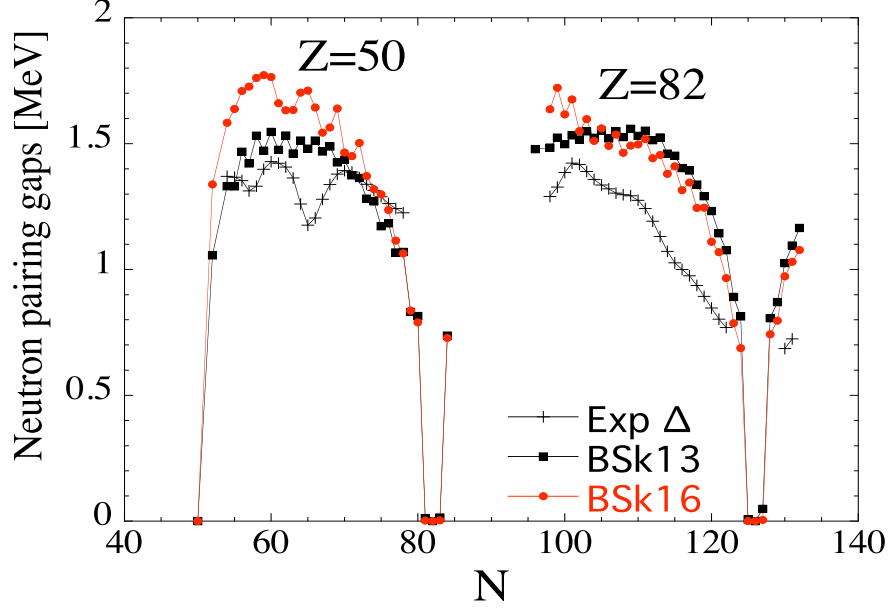


FIG. 4: Comparison of the experimental even-odd differences $\Delta^{(5)}$ with the HFB-16 theoretical neutron spectral pairing gaps $\langle uv\Delta \rangle$ for the Sn and Pb isotopic chains.

level-density calculations with HFB-16, but Fig. 4 is encouraging.

Magic neutron-shell gaps. While the global fit to the mass data given by model HFB-16 is seen to be excellent, a few individual predictions could still be quite anomalous without having a serious impact on the global fit. Of particular importance in this respect are the masses involved in the definition of the neutron-shell gaps,

$$\Delta_n(N_0, Z) = S_{2n}(N_0, Z) - S_{2n}(N_0 + 2, Z) \quad , \quad (4.4)$$

In Figs. 5– 8 we show these gaps as a function of Z for the magic numbers $N_0 = 50, 82, 126$ and 184. The agreement with experiment is excellent for $N_0 = 50$ and 82, with strong gap quenching predicted as the neutron drip line is approached. On the other hand, for $N_0 = 126$ the agreement with experiment is quite bad, as is always the case with our HFB models. No quenching is predicted for either $N_0 = 126$ or 184.

Macroscopic properties. Table V shows the parameters of infinite and semi-infinite nuclear matter (INM and SINM) that we have calculated for the force BSk16 (for the definition of these parameters see, for example, Ref. [9]). Our SINM calculations, which do not take

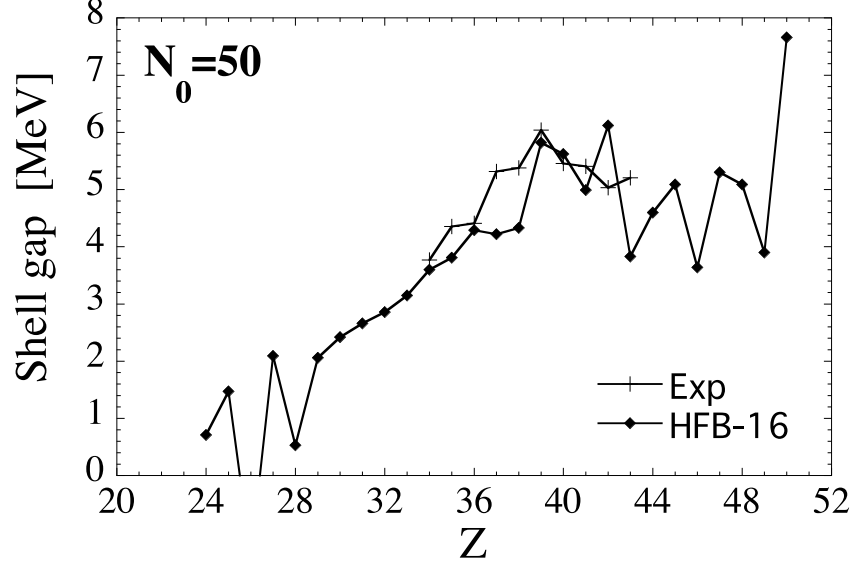


FIG. 5: $N_0 = 50$ shell gap as function of Z for mass model HFB-16.

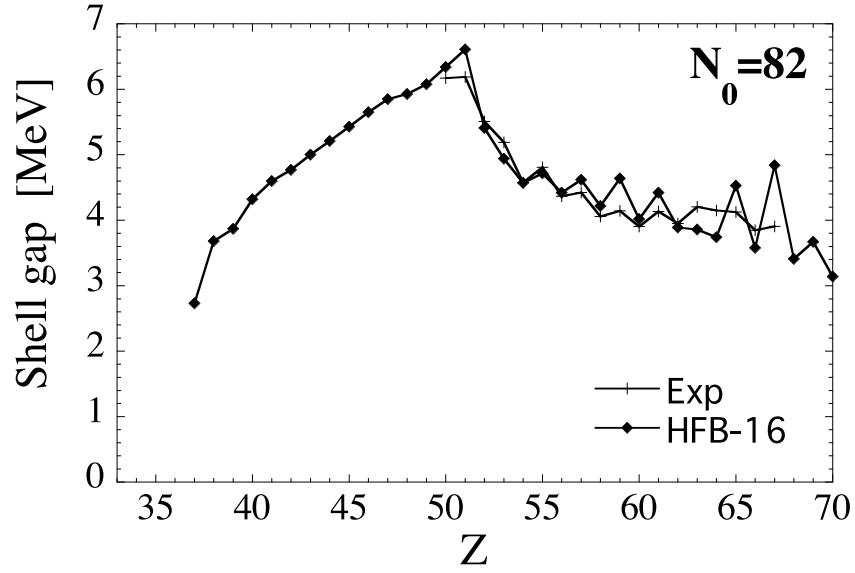


FIG. 6: $N_0 = 82$ shell gap as function of Z for mass model HFB-16.

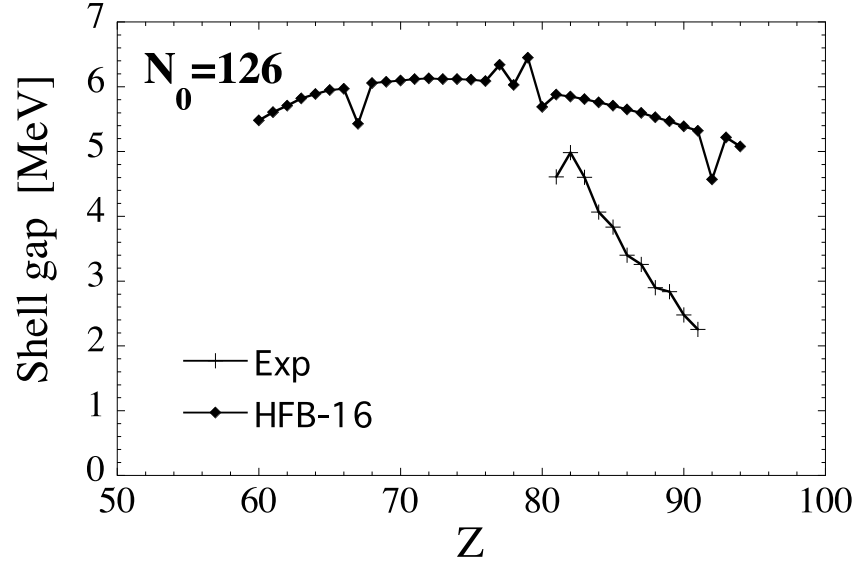


FIG. 7: $N_0 = 126$ shell gap as function of Z for mass model HFB-16.

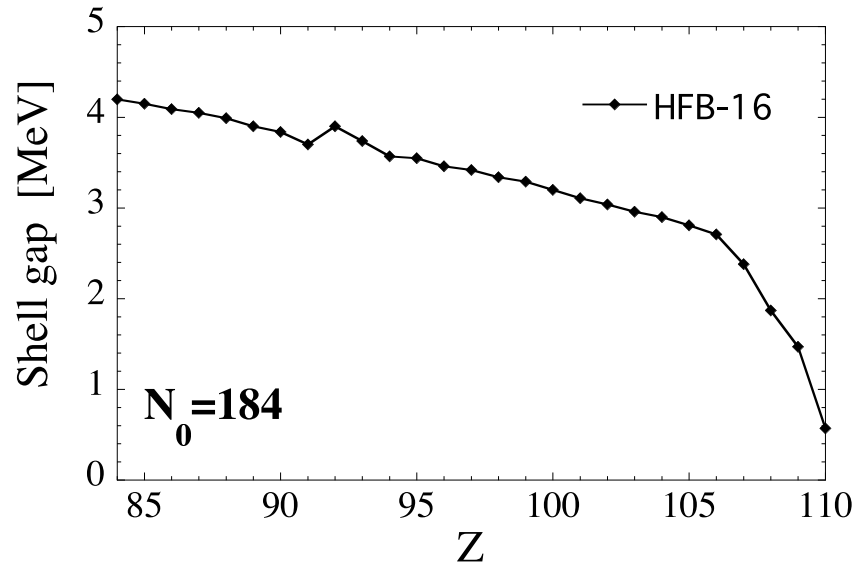


FIG. 8: $N_0 = 184$ shell gap as function of Z for mass model HFB-16.

pairing into account, are performed using the HF code of M. Farine, as described in Appendix A of Ref. [52]. It should be noted that the values of M_s^* and J were imposed, as described at the beginning of this Section. In this table we show also the corresponding parameters for our last two forces; it will be seen that there has been very little change, although it is interesting to note that with the omission of Coulomb exchange (BSk15 and BSk16) the binding energy per nucleon of symmetric INM, a_v , has increased. All our values of these parameters are compatible with all the available experimental data, as discussed in Ref. [9]. To this earlier discussion we would like to append the remark that with all our forces we find an isovector effective mass M_v^* that is smaller than the isoscalar effective mass M_s^* at the density ρ_0 . This result implies that the neutron effective mass M_n^* is larger than the proton effective mass M_p^* in neutron-rich matter. Such an isovector splitting of the effective mass is consistent with measurements of isovector giant resonances [53], and has been confirmed in several many-body calculations with realistic forces [54, 55].

The energy-density curve of neutron matter for force BSk16 is indistinguishable from the realistic curve of Ref. [13] up to the supernuclear density of $0.3 \text{ neutron.fm}^{-3}$, as is the case with all our other forces that have been fitted to $J = 30 \text{ MeV}$, i.e, BSk9 and all later forces (see Fig. 13 of Ref. [9]). It is to be noted that unlike Ref. [53] we have not had to resort to a second t_3 term in the Skyrme force in order to simultaneously fit neutron matter and obtain the correct sign for the isovector splitting of the effective mass.

Fig. 9 shows the potential energy per particle in each of the four two-body spin-isospin (S, T) channels as a function of density for symmetric INM; we give results for both BSk16 and Brueckner-Hartree-Fock (BHF) calculations with realistic two- and three-nucleon forces. These latter results are taken from Fig. 6 of Ref. [53] and quoted as Ref. 62 of that paper. There is reasonable agreement between BSk16 and the realistic calculations in all states except the (1,1) state, where BSk16 is strongly attractive, while BHF is very weak. It seems to be very difficult, in fact, to fit both odd states with a conventional Skyrme force. For example, SLy4 [37] handles the (1,1) state rather well, having imposed $x_2 = -1$, but as a result works much worse than BSk16 for the (0,0) state. In any case, the excessive attraction that BSk16 gives in the (1,1) state leads to the onset of a ferromagnetic instability in neutron matter at relatively low density, as seen from the value of ρ_{fmg}/ρ_0 in Table V.

Stability of extrapolation. Although all our models agree fairly closely in the known region of the nuclear chart, simply by virtue of their fit to the data, there is no *a priori* guarantee

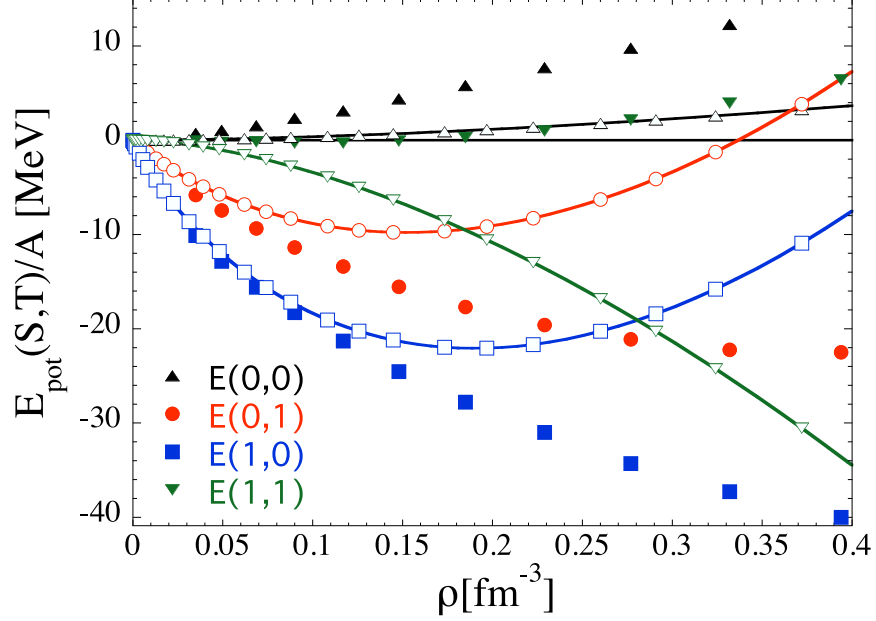


FIG. 9: Potential energy per particle in each (S, T) channel as a function of density for symmetric INM. The full symbols correspond to BHF calculations and the open symbols (connected with solid lines) to the BSk16 force.

that they will give comparable extrapolations to the astrophysically interesting region close to the neutron drip line. Accordingly, in Table VI we compare the predictions made by HFB-16 with our earlier models HFB-15, HFB-14 and HFB-8 for all those nuclei with $26 \leq Z \leq 110$ for which $S_n < 4.0$ MeV. This table shows that for the more astrophysically relevant quantities S_n and Q_β the differences between the various model predictions are much smaller than for the absolute masses, and in fact are comparable to the deviations between each model and the data. This stability of the predictions against slight changes in the model is consistent with an overall reliability of the HFB approach, although insofar as differences between the model predictions are significant, we would prefer HFB-16, given both the excellence of its fit to the data and the high degree of reality built into the model. In this latter respect, the conformity of both the Skyrme and pairing components of the effective force to realistic neutron-matter calculations should particularly enhance our confidence in predictions for highly neutron-rich nuclei.

V. CONCLUSIONS

The new feature that we introduce here in this latest of our series of Skyrme-HFB mass models, HFB-16, is the requirement that the contact pairing force reproduce exactly at each density encountered in the nuclear system (nucleus or the inner crust of neutron stars) the 1S_0 pairing gap of neutron matter, as determined in microscopic calculations with realistic nucleon-nucleon forces. We retain the earlier constraints on the Skyrme force of reproducing the energy-density curve of neutron matter, and of having an isoscalar effective mass of $0.8M$ in symmetric INM at the saturation density ρ_0 ; we also keep the recently adopted device of dropping Coulomb exchange. Furthermore, the correction term for the spurious energy of collective motion has a form that is known to favour fission barriers that are in good agreement with experiment.

Remarkably, despite the severe constraints imposed by neutron matter on both the Skyrme and pairing components of the effective force we have achieved the best fit ever to the mass data within the framework of mean-field models (the improvement is particularly striking for the most neutron-rich nuclei). The rms error σ of the 2149 measured masses of nuclei with N and $Z \geq 8$ has been reduced to 0.632 MeV. Very few other mean-field mass tables have been published, the most successful of which is the RMF table of Ref. [16], the rms error for essentially all measured nuclei being 2.1 MeV. Also to be noted is the mass table based on the SLy4 Skyrme force; this is limited to even-even nuclei and gives $\sigma = 5.1$ MeV [38, 39]. Turning to models lacking the microscopic basis of self-consistent mean-field models, we note that for the FRDM (“finite-range droplet model”) [56] $\sigma = 0.656$ MeV, while for the Duflo-Zuker model [57] we have $\sigma = 0.360$ MeV (these last two values of σ are both for 2149 nuclei). Only this last model does better than we do with the model presented here, but its applicability is limited to masses: it cannot be extended to any of the other quantities of astrophysical interest, such as fission barriers or the properties of the inner crust of neutron stars.

Not only is our model well adapted to the determination of these quantities, it turns out that even with no flexibility at all remaining for the pairing force, the spectral pairing gaps that we find suggest that level densities in good agreement with experiment should be obtained. Finally, we find the correct sign for the isovector effective mass splitting without introducing additional terms in the effective force.

Much of the success of the present model must lie with the new constraint that we have imposed, i.e., our scheme for *exactly* matching the effective density-dependent contact pairing force to realistic microscopic calculations on neutron matter. We suspect also that a crucial role was played by the decision to make the pairing force for nucleons of charge type q depend only on ρ_q . The modification of the collective correction (4.2) has also contributed significantly to the improvement. (Dropping Coulomb exchange certainly accounts in part for the superiority of HFB-16 over HFB-14 and earlier models.)

It is noteworthy that widely differing neutron-matter gaps can still correspond to the same finite-nucleus gaps, as well illustrated by the gaps for forces BSk7, BSk8 and BSk16 shown in Fig.1, all of which lead to comparably good mass fits. This flexibility originates in the crucial role that the Skyrme force plays in passing from neutron-matter gaps to finite-nucleus gaps. It is this flexibility which allowed us to successfully impose the additional constraint of fitting to the neutron-matter gaps. On the other hand, it does not follow that one can start with any neutron-matter gap: for example, when we took screened neutron-matter gaps as our starting point we were unable to get good mass fits, no matter how the Skyrme force was adjusted. The fact that we do get better mass fits while neglecting medium effects suggests that these effects might be compensated in finite nuclei by, for example, coupling of particles via surface vibrations. Alternatively, the nuclear-matter medium effects themselves might be rather small, as indicated by recent quantum Monte Carlo calculations [32, 33, 34, 35].

To summarize, the HFB16 mass model not only gives a better fit to the mass data than any other mean-field model, but is also by far the most microscopically founded. It can thus be expected to make more reliable predictions of the highly neutron-rich nuclei of astrophysical interest. In particular, this is the first of our models well adapted to the investigation of a possible superfluid phase in the inner crust of neutron stars; in this respect it should be realized that since the model reproduces with precision all the mass data it must be giving a good account of surface properties, an important point in dealing with the inhomogeneities of the crust.

Acknowledgments

We are grateful to M. Bender and T. Duguet for valuable communications. M. Farine is thanked for allowing us to use his HF code for semi-infinite nuclear matter. The financial

support of the FNRS (Belgium) and the NSERC (Canada) is acknowledged. N.C. is grateful for the award of a Marie Curie Intra-European fellowship (contract number MEIF-CT-2005-024660).

APPENDIX A: RELATION BETWEEN DIFFERENT FORMULATIONS OF THE HFB METHOD

Computation of the HFB matrix elements. Our main concern in this appendix is to show how the computation of the oscillator matrix elements (2.11a) and (2.11b) is greatly facilitated by starting with a density functional of the general form given by Eq. (2.16), and working in coordinate space. First, however, we recall the definitions and various properties of the quantities appearing in this last equation.

We have introduced

(i) the nucleon density,

$$\rho_q(\mathbf{r}) = \sum_{\sigma=\pm 1} \rho_q(\mathbf{r}, \sigma; \mathbf{r}, \sigma), \quad (\text{A.1})$$

(ii) the kinetic-energy density (in units of $\hbar^2/2M_q$),

$$\tau_q(\mathbf{r}) = \sum_{\sigma=\pm 1} \int d^3\mathbf{r}' \delta(\mathbf{r} - \mathbf{r}') \nabla \cdot \nabla' \rho_q(\mathbf{r}, \sigma; \mathbf{r}', \sigma) \quad (\text{A.2})$$

(iii) the spin-current density,

$$\begin{aligned} \mathbf{J}_q(\mathbf{r}) &= -i \sum_{\sigma, \sigma'=\pm 1} \int d^3\mathbf{r}' \delta(\mathbf{r} - \mathbf{r}') \nabla \rho_q(\mathbf{r}, \sigma; \mathbf{r}', \sigma') \times \boldsymbol{\sigma}_{\sigma'\sigma} \\ &= i \sum_{\sigma, \sigma'=\pm 1} \int d^3\mathbf{r}' \delta(\mathbf{r} - \mathbf{r}') \nabla' \rho_q(\mathbf{r}, \sigma; \mathbf{r}', \sigma') \times \boldsymbol{\sigma}_{\sigma'\sigma} \end{aligned} \quad (\text{A.3})$$

and (iv) the so-called local pairing density [24, 25]

$$\tilde{\rho}_q(\mathbf{r}) = \sum_{\sigma=\pm 1} \tilde{\rho}_q(\mathbf{r}, \sigma; \mathbf{r}, \sigma), \quad (\text{A.4})$$

where $\boldsymbol{\sigma}_{\sigma\sigma'}$ denotes the Pauli spin matrices, $\rho(\mathbf{r}, \sigma; \mathbf{r}', \sigma')$ and $\tilde{\rho}_q(\mathbf{r}, \sigma; \mathbf{r}, \sigma)$ are the normal and abnormal density matrices respectively, expressed in so-called coordinate space (position \mathbf{r} and spin state $\sigma = \pm 1$). From the general definitions of these two matrices [24, 25], it

follows that the relationship between the coordinate space representation and the discrete-basis representation given in Eqs. (2.7a) and (2.7b), respectively, is

$$\rho_q(\mathbf{r}, \sigma; \mathbf{r}', \sigma') = \sum_{ij(q)} \rho_{ij} \phi_i(\mathbf{r}, \sigma) \phi_j^*(\mathbf{r}', \sigma') \quad (\text{A.5a})$$

and

$$\tilde{\rho}_q(\mathbf{r}, \sigma; \mathbf{r}', \sigma') = -\sigma' \sum_{ij(q)} \kappa_{ij} \phi_i(\mathbf{r}, \sigma) \phi_j(\mathbf{r}', -\sigma'), \quad (\text{A.5b})$$

where $\phi_i(\mathbf{r}, \sigma)$ denote the s.p. basis wave functions.

We return now to the question of the oscillator matrix elements (2.11a) and (2.11b). Remarking that E_{HFB} is a functional of $\rho_q(\mathbf{r})$ (and its gradient), $\tau_q(\mathbf{r})$, $\mathbf{J}_q(\mathbf{r})$ and $\tilde{\rho}_q(\mathbf{r})$, which in turn depend on the matrices ρ_{ij} and κ_{ij} , we have

$$\begin{aligned} h'_{ij} &\equiv \frac{\partial E_{\text{HFB}}}{\partial \rho_{ji}} \\ &= \int d^3\mathbf{r} \left[\frac{\delta E_{\text{HFB}}}{\delta \rho_q(\mathbf{r})} \frac{\partial \rho_q(\mathbf{r})}{\partial \rho_{ji}} + \frac{\partial \mathcal{E}_{\text{HFB}}(\mathbf{r})}{\partial \tau_q(\mathbf{r})} \frac{\partial \tau_q(\mathbf{r})}{\partial \rho_{ji}} + \frac{\partial \mathcal{E}_{\text{HFB}}(\mathbf{r})}{\partial \mathbf{J}_q(\mathbf{r})} \cdot \frac{\partial \mathbf{J}_q(\mathbf{r})}{\partial \rho_{ji}} \right] \end{aligned} \quad (\text{A.6a})$$

and

$$\Delta_{ij} \equiv \frac{\partial E_{\text{HFB}}}{\partial \kappa_{ij}^*} = \int d^3\mathbf{r} \frac{\partial \mathcal{E}_{\text{HFB}}(\mathbf{r})}{\partial \tilde{\rho}_q(\mathbf{r})} \frac{\partial \tilde{\rho}_q(\mathbf{r})}{\partial \kappa_{ij}^*}, \quad (\text{A.6b})$$

where we have introduced the functional derivative

$$\frac{\delta E_{\text{HFB}}}{\delta \rho_q(\mathbf{r})} \equiv \frac{\partial \mathcal{E}_{\text{HFB}}(\mathbf{r})}{\partial \rho_q(\mathbf{r})} - \nabla \cdot \frac{\partial \mathcal{E}_{\text{HFB}}(\mathbf{r})}{\partial \nabla \rho_q(\mathbf{r})}. \quad (\text{A.7})$$

Substituting Eqs. (A.1) -(A.3) into Eq. (A.6a), together with Eqs. (A.5a), yields

$$h'_{ij} = \sum_{\sigma, \sigma' = \pm 1} \int d^3\mathbf{r} \phi_i^*(\mathbf{r}\sigma') h'_q(\mathbf{r})_{\sigma'\sigma} \phi_j(\mathbf{r}\sigma), \quad (\text{A.8})$$

in which $h'_q(\mathbf{r})_{\sigma\sigma'} = \sigma\sigma' h'_q(\mathbf{r})_{-\sigma' -\sigma}^*$ is the self-consistent s.p Hamiltonian, appearing in the coordinate-space form of the HFB equations (A.18)

$$h'_q(\mathbf{r})_{\sigma'\sigma} \equiv -\nabla \cdot \frac{\hbar^2}{2M_q^*(\mathbf{r})} \nabla \delta_{\sigma\sigma'} + U_q(\mathbf{r}) \delta_{\sigma\sigma'} - i\mathbf{W}_q(\mathbf{r}) \cdot \nabla \times \boldsymbol{\sigma}_{\sigma'\sigma} \quad (\text{A.9})$$

where

$$\frac{\hbar^2}{2M_q^*(\mathbf{r})} = \frac{\partial \mathcal{E}_{\text{HFB}}(\mathbf{r})}{\partial \tau_q(\mathbf{r})}, \quad U_q(\mathbf{r}) = \frac{\delta E_{\text{HFB}}}{\delta \rho_q(\mathbf{r})}, \quad \mathbf{W}_q(\mathbf{r}) = \frac{\partial \mathcal{E}_{\text{HFB}}(\mathbf{r})}{\partial \mathbf{J}_q(\mathbf{r})}. \quad (\text{A.10})$$

To reduce Eq. (A.6b) in the same way requires that we make use of Eqs. (A.4) and (A.5b), and also the expression

$$\phi_{\bar{i}}(\mathbf{r}, \sigma) \equiv -i\sigma_y \phi_i^*(\mathbf{r}, \sigma) = -\sigma \phi_i^*(\mathbf{r}, -\sigma) \quad (\text{A.11})$$

for the time-reversed conjugate $\phi_{\bar{i}}(\mathbf{r}, \sigma)$ of the s.p. state $\phi_i(\mathbf{r}, \sigma)$. In this way we find

$$\Delta_{ij} = \sum_{\sigma=\pm 1} \int d^3\mathbf{r} \phi_i^*(\mathbf{r}\sigma) \Delta_q(\mathbf{r}) \phi_{\bar{j}}(\mathbf{r}\sigma), \quad (\text{A.12})$$

in which $\Delta_q(\mathbf{r})$ is the self-consistent local pairing potential, appearing in the coordinate-space form of the HFB equations (A.18)

$$\Delta_q(\mathbf{r}) \equiv \frac{\partial \mathcal{E}_{\text{HFB}}(\mathbf{r})}{\partial \tilde{\rho}_q(\mathbf{r})}; \quad (\text{A.13})$$

this must be real if time-reversibility holds, since $\tilde{\rho}_q(\mathbf{r})$ will then be real [24, 25].

Explicit expressions for the fields appearing in Eqs. (A.10) and (A.13) are as follows.

$$\begin{aligned} \frac{\hbar^2}{2M_q^*} = \frac{\partial \mathcal{E}_{\text{HFB}}}{\partial \tau_q} = \frac{\hbar^2}{2M_q} + \frac{1}{4}t_1 \left[\left(1 + \frac{1}{2}x_1\right) \rho - \left(\frac{1}{2} + x_1\right) \rho_q \right] \\ + \frac{1}{4}t_2 \left[\left(1 + \frac{1}{2}x_2\right) \rho + \left(\frac{1}{2} + x_2\right) \rho_q \right], \end{aligned} \quad (\text{A.14})$$

$$\begin{aligned} U_q &= \frac{\delta E_{\text{HFB}}}{\delta \rho_q} = \frac{\partial \mathcal{E}_{\text{HFB}}}{\partial \rho_q} - \nabla \cdot \frac{\partial \mathcal{E}_{\text{HFB}}}{\partial (\nabla \rho_q)} \\ &= t_0 \left[\left(1 + \frac{1}{2}x_0\right) \rho - \left(\frac{1}{2} + x_0\right) \rho_q \right] \\ &+ \frac{1}{4}t_1 \left[\left(1 + \frac{1}{2}x_1\right) \left(\tau - \frac{3}{2}\nabla^2 \rho\right) - \left(\frac{1}{2} + x_1\right) \left(\tau_q - \frac{3}{2}\nabla^2 \rho_q\right) \right] \\ &+ \frac{1}{4}t_2 \left[\left(1 + \frac{1}{2}x_2\right) \left(\tau + \frac{1}{2}\nabla^2 \rho\right) + \left(\frac{1}{2} + x_2\right) \left(\tau_q + \frac{1}{2}\nabla^2 \rho_q\right) \right] \\ &+ \frac{1}{12}t_3 \left[\left(1 + \frac{1}{2}x_3\right) (2 + \gamma)\rho^{\gamma+1} - \left(\frac{1}{2} + x_3\right) \left(2\rho^\gamma \rho_q + \gamma\rho^{\gamma-1} \sum_{q'=n,p} \rho_{q'}^2\right) \right] \\ &- \frac{1}{2}W_0 (\nabla \cdot \mathbf{J} + \nabla \cdot \mathbf{J}_q) + \delta_{q,p} V^{\text{Coul}} + \frac{1}{4} \sum_{q'=n,p} \frac{\partial v^{\pi q'}}{\partial \rho_q} \tilde{\rho}_{q'}^2 \end{aligned} \quad (\text{A.15})$$

and

$$\mathbf{W}_q = \frac{\partial \mathcal{E}_{\text{HFB}}}{\partial \mathbf{J}_q} = \frac{1}{2}W_0 \nabla (\rho + \rho_q) - \frac{1}{8}(t_1 x_1 + t_2 x_2) \mathbf{J} + \frac{1}{8}(t_1 - t_2) \mathbf{J}_q. \quad (\text{A.16})$$

Note that for the Coulomb field term $\delta_{q,p}V^{\text{Coul}}$ appearing in Eq. (A.15) we have taken the electrostatic potential given by Eq. (2.18), which, in view of the finite proton size, is not given exactly by the functional derivative of the Coulomb energy $(\delta E_{\text{Coul}})/(\delta \rho_p)$.

The local pairing field, defined in Eq. (A.13), is given by

$$\Delta_q = \frac{\partial \mathcal{E}_{\text{HFB}}}{\partial \tilde{\rho}_q} = \frac{1}{2} v^{\pi q} [\rho_n, \rho_p] \tilde{\rho}_q. \quad (\text{A.17})$$

Let us point out that the pairing functional $\mathcal{E}_{\text{pair}}$ contributes not only to this pairing field but also, through its dependence on the nucleon density, to the s.p. Hamiltonian $h'_q(\mathbf{r})_{\sigma\sigma'}$ as the last term of Eq. (A.15), which is essentially a rearrangement term, corresponding to the second term of Eq. (2.14). (All the other rearrangement field terms, corresponding to the first term of Eq. (2.14), appear in Eq. (A.15), and can be identified by their coefficient $t_3\gamma$.)

Transformation from discrete-basis to coordinate-space formulations of HFB equations.

It is convenient now to point out that the HFB equations in coordinate space can be obtained directly from the standard formulation of Refs. [19, 20], i.e., from the corresponding equations in discrete-basis form (2.10), by substituting in the latter Eqs. (A.8) and (A.12), and invoking time-reversibility.

This leads for each nucleon species q to the coordinate-space form of these equations, as given by Refs. [24, 25], thus

$$\sum_{\sigma'=\pm 1} \begin{pmatrix} h'_q(\mathbf{r})_{\sigma\sigma'} - \lambda_q \delta_{\sigma\sigma'} & \Delta_q(\mathbf{r}) \delta_{\sigma\sigma'} \\ \Delta_q(\mathbf{r}) \delta_{\sigma\sigma'} & -h'_q(\mathbf{r})_{\sigma\sigma'} + \lambda_q \delta_{\sigma\sigma'} \end{pmatrix} \begin{pmatrix} \psi_{1i}^{(q)}(\mathbf{r}, \sigma') \\ \psi_{2i}^{(q)}(\mathbf{r}, \sigma') \end{pmatrix} = E_i \begin{pmatrix} \psi_{1i}^{(q)}(\mathbf{r}, \sigma) \\ \psi_{2i}^{(q)}(\mathbf{r}, \sigma) \end{pmatrix}, \quad (\text{A.18})$$

where the s.p. Hamiltonian $h'_q(\mathbf{r})_{\sigma\sigma'}$ and pairing field $\Delta_q(\mathbf{r})$ for the forces (2.1) and (2.2) are as given in Appendix A (note that the rearrangement terms are included here). The upper and lower components of the Bogoliubov quasiparticle wave function, denoted respectively by $\psi_{1i}^{(q)}(\mathbf{r}, \sigma)$ and $\psi_{2i}^{(q)}(\mathbf{r}, \sigma)$, are related to the U and V matrices introduced in Eq. (2.5) by

$$\psi_{1i}^{(q)}(\mathbf{r}, \sigma) = \sum_{j(q)} U_{ji} \phi_j(\mathbf{r}, \sigma), \quad \psi_{2i}^{(q)}(\mathbf{r}, \sigma) = \sum_{j(q)} V_{ji} \phi_{\bar{j}}(\mathbf{r}, \sigma); \quad (\text{A.19})$$

note the appearance of the time-reversed conjugate state in the latter expression (Eq. (6) of Ref [58] is wrong).

Using Eqs. (A.19), (A.5a), (A.5b) and the assumed time-reversal invariance, we have the

identities

$$\rho_q(\mathbf{r}, \sigma; \mathbf{r}', \sigma') = \sum_{i(q)} \psi_{2i}^{(q)}(\mathbf{r}, \sigma) \psi_{2i}^{(q)}(\mathbf{r}', \sigma')^* \quad (\text{A.20})$$

and

$$\tilde{\rho}_q(\mathbf{r}, \sigma; \mathbf{r}', \sigma') = - \sum_{i(q)} \psi_{2i}^{(q)}(\mathbf{r}, \sigma) \psi_{1i}^{(q)}(\mathbf{r}', \sigma')^* = - \sum_i \psi_{1i}^{(q)}(\mathbf{r}, \sigma) \psi_{2i}^{(q)}(\mathbf{r}', \sigma')^*. \quad (\text{A.21})$$

Applying the properties of the U and V matrices, as given for example by Eqs. (7.5) of Ref. [20], to the definition (A.19) it can be easily checked that the quasiparticle wavefunction satisfies the completeness relations given by Eqs. (2.20a) and (2.20b) of Ref. [24].

APPENDIX B: HFB EQUATIONS IN UNIFORM MATTER

In a uniform system, it is natural to replace the oscillator basis by a plane-wave basis,

$$\phi_k(\mathbf{r}, \sigma) \equiv \frac{1}{\sqrt{\mathcal{V}}} \exp(i\mathbf{k} \cdot \mathbf{r}) \chi(\sigma), \quad (\text{B.1})$$

where $\chi(\sigma)$ is the Pauli spinor and \mathcal{V} is the normalization volume. It is easily seen from Eq. (A.8) that the s.p. Hamiltonian $h'_q(\mathbf{r})_{\sigma\sigma'}$ is diagonal in this basis,

$$h'_{kl} = \varepsilon_k^{(q)} \delta_{kl}, \quad (\text{B.2})$$

with

$$\varepsilon_k^{(q)} = \frac{\hbar^2 k^2}{2M_q^*} + U_q. \quad (\text{B.3})$$

Also, since the pairing field $\Delta_q(\mathbf{r})$ must be independent of \mathbf{r} in a uniform system it follows from Eq. (A.12) that all matrix elements Δ_{lk} vanish unless $l = \bar{k}$, i.e.,

$$\Delta_{lk} = \delta_{l\bar{k}} \Delta_q = -\Delta_{kl} \quad (\text{B.4})$$

where Δ_q is a constant for a given uniform system at a given density, given by Eq. (A.17). The assumption that the pairing force acts only between states of the s.p. Hamiltonian that are the time-reversal of each other constitutes the essence of the BCS method (note that this approximation differs from that discussed in Ref. [25]), an approximation to the HFB method that is often convenient for finite nuclei, but we have shown here that for uniform

systems the HFB method reduces exactly to the BCS method. Furthermore, for infinite but inhomogeneous nuclear matter, the weaker the departure from homogeneity the better the BCS method will approximate the HFB method; this means that in the inner crust of neutron stars the BCS approximation will be better the deeper the layer in question.

More precisely, by inspecting Eq. (A.12) and by remembering that only s.p. states close to the Fermi level contribute to pairing correlations, it can be seen that in general the BCS approach is justified whenever the pairing field is slowly varying in the spatial domain for which the s.p. wavefunctions for states around the Fermi level, are non-vanishing. This condition is usually fulfilled for strongly bound nuclei (for which the chemical potential λ_q lies deep inside the s.p. potential well) since the pairing field $\Delta_q(\mathbf{r})$ is typically more or less constant in the nuclear interior, where the bound s.p. wavefunctions take their largest values. In contrast, for weakly bound nuclei, pairing correlations involve not only bound states but also states from the continuum. Since the pairing field vanishes outside the nucleus, it follows that it will be varying rapidly in a region where the s.p. states that contribute to pairing are still strong, whence the BCS approximation can be expected to break down for such nuclei.

Solving now the HFB equations (2.10) by using Eqs. (B.2) and (B.4) yields

$$E_k^{(q)} = \sqrt{(\varepsilon_k^{(q)} - \lambda_q)^2 + \Delta_q^2}, \quad (\text{B.5a})$$

$$U_{kk}^{(q)} = U_{\bar{k}\bar{k}}^{(q)} = \frac{1}{\sqrt{2}} \left(1 + \frac{\varepsilon_k^{(q)} - \lambda_q}{E_k^{(q)}} \right)^{1/2} \quad (\text{B.5b})$$

and

$$V_{k\bar{k}}^{(q)} = -V_{\bar{k}k}^{(q)} = \frac{1}{\sqrt{2}} \left(1 - \frac{\varepsilon_k^{(q)} - \lambda_q}{E_k^{(q)}} \right)^{1/2}, \quad (\text{B.5c})$$

making use of the properties of the U and V matrices. Using Eq. (A.19), (B.5b) and (B.5c) it can be seen that the quasiparticle wavefunction in uniform nuclear matter reduces to

$$\psi_{1k}^{(q)}(\mathbf{r}, \sigma) = U_{kk}^{(q)} \phi_k(\mathbf{r}, \sigma), \quad \psi_{2k}^{(q)}(\mathbf{r}, \sigma) = V_{\bar{k}k}^{(q)} \phi_k(\mathbf{r}, \sigma), \quad (\text{B.6})$$

where $\phi_k(\mathbf{r}, \sigma)$ is given by Eq. (B.1).

Substituting Eqs. (B.5b) and (B.5c) in Eqs. (2.7a) and (2.7b) leads to the familiar expressions of the normal and abnormal density matrices

$$\rho_{kl} = (V_{k\bar{k}})^2 \delta_{kl}, \quad \kappa_{kl} = V_{k\bar{k}} U_{kk} \delta_{\bar{k}l}. \quad (\text{B.7})$$

Using Eq. (A.1) and (A.5a) together with (B.1) and (B.5c), the nucleon density $\rho_q(\mathbf{r}) \equiv \rho_q$ is given by

$$\rho_q = \frac{1}{4\pi^2} \left(\frac{2M_q^*}{\hbar^2} \right)^{3/2} \int_{U_q}^{+\infty} d\varepsilon \sqrt{\varepsilon} \left(1 - \frac{\varepsilon - \lambda_q}{\sqrt{(\varepsilon - \lambda_q)^2 + \Delta_q^2}} \right). \quad (\text{B.8})$$

Likewise from Eqs. (B.7) and (2.9b) we find the “BCS gap equation”

$$\Delta_q = -\frac{1}{8\pi^2} \left(\frac{2M_q^*}{\hbar^2} \right)^{3/2} v^{\pi q}[\rho_n, \rho_p] \Delta_q \int_{\Lambda} d\varepsilon \frac{\sqrt{\varepsilon}}{\sqrt{(\varepsilon - \lambda_q)^2 + \Delta_q^2}}. \quad (\text{B.9})$$

The integral is taken inside the subspace Λ introduced to regularize the ultra-violet divergences, arising from the zero range of the pairing interaction. These divergences are removed by imposing a cutoff, either in the q.p. energy spectrum or in the s.p. energy spectrum. In the latter case, different prescriptions have been employed in the literature: (i) $\varepsilon < \varepsilon_{\Lambda}$, (ii) $\varepsilon < U_q + \varepsilon_{\Lambda}$, (iii) $\varepsilon < \lambda_q + \varepsilon_{\Lambda}$, (iv) $\lambda_q - \varepsilon_{\Lambda} < \varepsilon < \lambda_q + \varepsilon_{\Lambda}$ where ε_{Λ} is a constant. The fixed cutoff (i) is the only choice which implies that the gap equations depend explicitly on the s.p. potential U_q . Since a density dependent pairing force affects directly the s.p. energies via the rearrangement potential (see Eq. (A.15)), the gap equations (B.9) will involve not only the pairing strength $v^{\pi q}[\rho_n, \rho_p]$ but also its partial derivatives. Note that since the integrand in the integral appearing in Eq. (B.9) takes significant values only in the vicinity of the Fermi level, the cutoff prescriptions (i) and (ii) lead to essentially zero pairing gaps $\Delta_q \simeq 0$ for densities such that $\varepsilon_{\Lambda} < \lambda_q$ and $\varepsilon_{\Lambda} < \mu_q$ respectively. A peculiar consequence is that the pairing gap may be vanishingly small while the pairing force is not. We have encountered such a situation for the Skyrme force SLy4 with the pairing force of Ref. [39] using the cutoff prescription (i), as can be seen by comparing Figs. 1 and 2.

-
- [1] M. Arnould, S. Goriely, K. Takahashi, Phys. Reports 450 (2007) 97.
 - [2] P. Haensel, A. Y. Potekhin, D. G. Yakovlev, Neutron Stars 1: Equation of state and structure, Springer (2007), chapter 3.
 - [3] M. Samyn, S. Goriely, P.-H. Heenen, J.M. Pearson, F. Tondeur, Nucl. Phys. A700 (2002) 142.
 - [4] S. Goriely, M. Samyn, P.-H. Heenen, J.M. Pearson, F. Tondeur, Phys. Rev. C 66 (2002) 024326.

- [5] M. Samyn, S. Goriely, J.M. Pearson, Nucl. Phys. A725 (2003) 69.
- [6] S. Goriely, M. Samyn, M. Bender, J. M. Pearson, Phys. Rev. C 68 (2003) 054325.
- [7] M. Samyn, S. Goriely, M. Bender, J.M. Pearson, Phys. Rev. C 70 (2004) 044309.
- [8] S. Goriely, M. Samyn, J. M. Pearson, and M. Onsi, Nucl. Phys. A750 (2005) 425.
- [9] S. Goriely, M. Samyn, J.M. Pearson, Nucl. Phys. A773 (2006) 279.
- [10] S. Goriely, M. Samyn, J.M. Pearson, Phys. Rev C 75 (2007) 064312.
- [11] S. Goriely and J. M. Pearson Phys. Rev. C 77 (2008) 031301(R).
- [12] G. Audi, A. H. Wapstra, C. Thibault, Nucl. Phys. A729 (2003) 337.
- [13] B. Friedman, V. R. Pandharipande, Nucl. Phys. A361 (1981) 502.
- [14] S. Hilaire, S. Goriely, Nucl. Phys. A779 (2006) 63.
- [15] G. A. Lalazissis, S. Raman, P. Ring, At. Data Nucl. Data Tables, 71 (1999) 1.
- [16] L. Geng, H. Toki, J. Meng, Prog. Theor. Phys. 113 (2005) 785.
- [17] J. M. Pearson, Phys. Lett. B513 (2001) 319.
- [18] T. Duguet, Phys. Rev. C 69 (2004) 054317.
- [19] H. J. Mang, Phys. Rep. 18C (1975) 325.
- [20] P. Ring, P. Schuck, *The Nuclear Many-Body Problem*, Springer, New York, 1980.
- [21] M. Farine, J. M. Pearson and F. Tondeur, Nucl. Phys. A696 (2001) 396.
- [22] W. Kohn, L. J. Sham, Phys. Rev. 140 (1966), A1133.
- [23] J.C. Slater, Phys. Rev. 81 (1951), 385.
- [24] J. Dobaczewski, H. Flocard, J. Treiner, Nucl. Phys. A422 (1984) 103.
- [25] J. Dobaczewski, W. Nazarewicz, T.R. Werner, J.F. Berger, C.R. Chinn, J. Dechargé, Phys. Rev. C 53 (1996), 2809.
- [26] D. Vautherin, Phys. Rev.C 7 (1973), 296.
- [27] E. Garrido, P. Sarriguren, E. Moya de Guerra, P. Schuck, Phys. Rev.C 60 (1999), 064312.
- [28] U. Lombardo and H. J. Schulze, “Superfluidity in neutron star matter” in LNP Vol. 578: Physics of Neutron Star Interiors, ed. D. Blaschke, N. K. Glendenning and A. Sedrakian, Springer (2001), 30.
- [29] D.J. Dean, M. Hjorth-Jensen, Rev. Mod. Phys. 75 (2003), 607.
- [30] M. Baldo, E.E. Saperstein, S.V. Tolokonnikov, Nucl. Phys. A 749 (2005) 42c.
- [31] Ø. Elgarøy, M. Hjorth-Jensen, Phys. Rev. C 57 (1998), 1174.
- [32] A. Fabrocini, S. Fantoni, A.Y. Illarionov, K. E. Schmidt, Phys. Rev. Lett. 95 (2005) 192501.

- [33] T. Abe, and R. Seki, arXiv preprint:nucl-th/0708.2523.
- [34] A. Gezerlis, J. Carlson, Phys. Rev. C 77 (2008) 032801.
- [35] S. Gandolfi, A. Yu. Illarionov, S. Fantoni, F. Pederiva, K. E. Schmidt, arXiv preprint 0805.2513.
- [36] A.D. Kaminker, P. Haensel, D.G. Yakovlev, Astron. and Astrophys. 373 (2001) L17.
- [37] E. Chabanat, P. Bonche, P. Haensel, J. Meyer, R. Schaeffer, Nucl. Phys. A 635 (1998) 231; Nucl. Phys. A 643 (1998) 441.
- [38] M.V. Stoitsov, J. Dobaczewski, W. Nazarewicz, S. Pittel, and D.J. Dean, Phys. Rev. C 68 (2003) 054312.
- [39] J. Dobaczewski, M.V. Stoitsov, W. Nazarewicz, AIP Conference Proceedings Volume 726, ed. R. Bijker, R.F. Casten, A. Frank (American Institute of Physics, New York, 2004) p. 51.
- [40] J. Margueron, H. Sagawa, K. Hagino, Phys. Rev.C 76 (2007), 064316.
- [41] J. Margueron, H. Sagawa, K. Hagino, Phys. Rev.C 77 (2008), 054309.
- [42] A. Bulgac, Y. Yu, Phys. Rev. Lett. 88 (2002) 042504.
- [43] W. Satula, R. Wyss, Phys. Lett. B393 (1997) 1.
- [44] W. Satula, D. J. Dean, J. Gary, S. Mizutori, W. Nazarewicz, Phys. Lett. B407 (1997) 103.
- [45] W. Satula, R. Wyss, Nucl. Phys. A676 (2000) 120.
- [46] E. Wigner, Phys. Rev. 51 (1937) 106.
- [47] G. Colò, N. Van Giai, J. Meyer, K. Bennaceur, P. Bonche, Phys. Rev. C 70 (2004) 024307.
- [48] B. G. Todd-Rutel, J. Piekarewicz, Phys. Rev. Lett. 95 (2005) 122501.
- [49] I. Angeli, At. Data and Nucl. Data Tables 87 (2004) 185.
- [50] I. Sick, Phys. Lett. B576 (2003) 62.
- [51] J. W. Negele, Phys. Rev. C 1 (1970) 1260.
- [52] M. Samyn, S. Goriely, J.M. Pearson, Phys. Rev. C 72 (2005) 044316.
- [53] T. Lesinski, K. Bennaceur, T. Duguet, J. Meyer, Phys. Rev. C 74 (2006) 044315.
- [54] E. N. van Dalen, C. Fuchs, A. Faessler, Phys. Rev. Lett. 95 (2005) 022302.
- [55] W. Zuo, U. Lombardo, H.-J. Schulze, Z. H. Li, Phys. Rev. C 74 (2006) 014317.
- [56] P. Möller, J. R. Nix, W.D. Myers, W.J. Swiatecki, At. Data Nucl. Data Tables 59 (1995) 185.
- [57] J. Duflo, A. P. Zuker, Phys. Rev. C 52 (1995) R23.
- [58] M. Bender, P.-H. Heenen, P.-G. Reinhard, Rev. Mod. Phys. 75 (2003) 121.

TABLE I: Parameters of the analytical fit (3.2) for the BCS pairing gap in neutron matter extracted from Fig. 7 of Ref. [28] (the unit of length is fermi and the unit of energy is MeV).

Δ_0	k_1	k_2	k_3	k_{\max}
910.603	1.38297	1.57068	0.905237	1.57

TABLE II: Force BSk16: lines 1-10 show the Skyrme parameters, lines 11-14 the pairing parameters and the last four lines the Wigner parameters (see Section IV for further details).

t_0 [MeV fm ³]	-1837.23
t_1 [MeV fm ⁵]	383.521
t_2 [MeV fm ⁵]	-3.41736
t_3 [MeV fm ^{3+3γ]}	11523.0
x_0	0.432600
x_1	-0.824106
x_2	44.6520
x_3	0.689797
W_0 [MeV fm ⁵]	141.100
γ	0.3
f_n^-	1.06
f_p^+	0.99
f_p^-	1.05
ε_Λ [MeV]	16.0
V_W [MeV]	-2.60
λ	240
V'_W [MeV]	0.70
A_0	32

TABLE III: Parameters of collective correction for model HFB-16 (see Section IV for further details).

b (MeV)	0.8
c	10
d (MeV)	2.6
l	10
β_2^0	0.1

TABLE IV: Rms (σ) and mean ($\bar{\epsilon}$) deviations between data and predictions for model HFB-16; for convenience we also show models HFB-15 [11], HFB-14 [10] and HFB-8 [7]. The first pair of lines refers to all the 2149 measured masses M , the second pair to the masses M_{nr} of the subset of 185 neutron-rich nuclei with $S_n \leq 5.0$ MeV, the third pair to the neutron separation energies S_n (1988 measured values), the fourth pair to beta-decay energies Q_β (1868 measured values) and the fifth pair to charge radii (782 measured values). The last line shows the calculated neutron-skin thickness of ^{208}Pb for these models.

	HFB-16	HFB-15	HFB-14	HFB-8
$\sigma(M)$ [MeV]	0.632	0.678	0.729	0.635
$\bar{\epsilon}(M)$ [MeV]	-0.001	0.026	-0.057	0.009
$\sigma(M_{nr})$ [MeV]	0.748	0.809	0.833	0.838
$\bar{\epsilon}(M_{nr})$ [MeV]	0.161	0.173	0.261	-0.025
$\sigma(S_n)$ [MeV]	0.500	0.588	0.640	0.564
$\bar{\epsilon}(S_n)$ [MeV]	-0.012	-0.004	-0.002	0.013
$\sigma(Q_\beta)$ [MeV]	0.559	0.693	0.754	0.704
$\bar{\epsilon}(Q_\beta)$ [MeV]	0.031	0.024	0.008	-0.027
$\sigma(R_c)$ [fm]	0.0313	0.0302	0.0309	0.0275
$\bar{\epsilon}(R_c)$ [fm]	-0.0149	-0.0108	-0.0117	0.0025
$\theta(^{208}\text{Pb})$ [fm]	0.15	0.15	0.16	0.12

TABLE V: Macroscopic parameters for force BSk16 (for convenience we also show forces BSk 15 [11] and BSk14 [10]). The first twelve lines refer to infinite nuclear matter, the last two to semi-infinite nuclear matter. See Section IV for further details.

	BSk16	BSk15	BSk14
a_v [MeV]	-16.053	-16.037	-15.853
ρ_0 [fm $^{-3}$]	0.1586	0.1589	0.1586
J [MeV]	30.0	30.0	30.0
M_s^*/M	0.80	0.80	0.80
M_v^*/M	0.78	0.77	0.78
K_v [MeV]	241.6	241.5	239.3
L [MeV]	34.87	33.60	43.91
G_0	-0.65	-0.67	-0.63
G'_0	0.51	0.54	0.51
G_1	1.52	1.47	1.49
G'_1	0.44	0.41	0.44
$\rho_{frm g}/\rho_0$	1.24	1.24	1.24
a_{sf} [MeV]	17.8	17.7	17.6
Q [MeV]	39.0	39.7	35.0

TABLE VI: Rms and mean differences between predictions for highly neutron-rich nuclei ($4.0 \text{ MeV} \geq S_n \geq 0$ and $26 \leq Z \leq 110$) given by different pairs of mass models. Mean differences are shown in parentheses.

	M	S_n	Q_β
HFB-15 - HFB-16	1.356 (0.977)	0.378 (-0.033)	0.520 (0.092)
HFB-14 - HFB-16	3.230(-2.465)	0.392 (0.136)	0.595 (-0.343)
HFB-8 - HFB-16	1.581 (0.319)	0.581 (-0.099)	0.892 (0.198)